Sensors & Transducers, Vol. 0, Issue 0, Month 2016, pp.

www.sensorsportal.com

Sensors & Transducers

http://www.sensorsportal.com

130nm CMOS SAR-ADC with Low Complexity Digital Control Logic

[1] M.Borgarino, [2] N.Verrascina, [2] J.B.Begueret

[1] Eng. Dept. "Enzo Ferrari", University of Modena and Reggio Emilia, Via Vivarelli 10, 41125 Modena, Italy

[2] University of Bordeaux, IMS Laboratory, 351 Cours de la Libération, 33400 Talence, France

[1] Tel.: +39 059 20561618, fax: +39 059 2056129

[1] E-mail: mattia.borgarino@unimore.it

Received: Accepted: Published:

Abstract: This paper reports on an original approach to design the digital control logic of a Successive Approximation Register Analog to Digital Converter, where no sequencers or code registers are used. It turns out a low complexity digital circuitry, which is applied to the design of a 130nm CMOS 8-bit SAR ADC. The simulations demonstrate that the proposed digital control logic correctly works leading to an Analog to Digital Converter exhibiting performances well aligned with the literature in terms of linearity, dissipated power, and energy spent per bit generation.

Keywords: SAR-ADC, control circuitry, CMOS, shift register, counter.

1. Introduction

The Successive Approximation Register Analog-to-Digital Converter (SAR-ADC), when compared with other ADC solutions (e.g. sigma-delta ADC, pipeline ADC), has its strengths in the low power consumption, medium-to-high resolution, and small form factor. Its weakness is in a high latency, as the conversion process requires operation cycles as many as the resolution. This mix of strengths and weakness makes the SAR-ADC very well suited for applications targeting low frequency signals and suffering from a limited energy availability. In medicine, the battery powering the integrated electronics front-end cannot be frequently replaced, because it is often implanted (e.g. pace-makers, heart defibrillators, epileptic seizure detector). In smart agriculture, the nodes of the sensor network distributed on a cultivation (e.g. vineyard) should work with a limited amount of available energy, because this energy should be harvested from the environment. Same consideration holds for the mobile sensors embedded in the collars for the smart monitoring of livestock (e.g. cow).

A SAR-ADC converts the value of the input analog signal, sampled at the given time, into a digital word generated after a given latency time elapsed from the sampling instant. The conversion process is based on a binary search algorithm, which explores a binary tree to find the best digital approximation, for a given resolution, of the input analog value. During the latency time the SAR-ADC explores this binary tree. The binary search algorithm is implemented in a digital control circuitry, which is usually constituted by sequencers and code registers [1]-[5], that makes complex the design flow. Aim of the present paper is to report on a low complexity approach to the design of the digital control circuitry [6]. The paper is organized as follows. Section 2 explains how the

binary search algorithm can be implemented, in order to simplify the design of the digital control circuitry. Section 3 focuses on the architecture and schematic of the proposed digital control circuitry. Section 4 applies the proposed digital control circuitry to the design of an 8-bit SAR-ADC in a bulk CMOS 130nm CMOS technology. Section 5 reports on the performances obtained for the designed SAR-ADC. Eventually, the paper ends with Section 6, where some conclusions are drawn.

2. Binary algorithm implementation

Figure 1 depicts the general architecture of a SAR-ADC. It is constituted by three main building blocks: the comparator, the Digital-to-Analog Converter (DAC), and the digital control circuitry, which is called hereinafter Digital Control Logic (DCL).

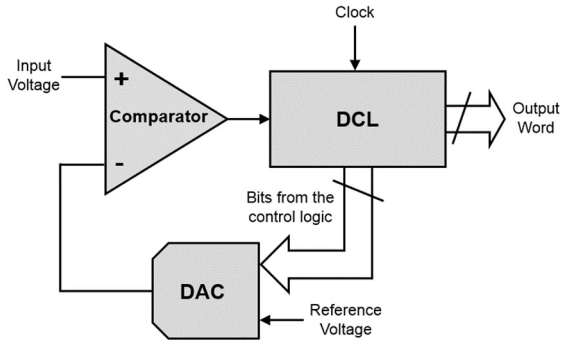

Fig. 1. General architecture of a SAR-ADC.

The present section addresses the implementation of the search binary algorithm run by the DCL. Generally speaking, the chosen implementation can make the design of the DCL more or less complex. In particular, in the present work the implementation was simplification orientated. For sake of clarity, a 4-bit resolution SAR-ADC is addressed.

The proposed approach moves from thinking of the DCL as a finite state machine, a point of view not adopted in the literature, even when the design sounds very close to a state transition diagram [2]. Figure 2 depicts the state transition diagram for the DCL, described as a finite state machine. It is worth noticing that the state diagram reproduces the structure of a binary tree. The diagram is distributed on four layers. The first layer is the initial state. In the fourth layer are the final states obtained at the end of the digitization process. The DCL goes through the states following the outcome of the comparator around which the SAR-ADC is designed (see Figure 1). Figure 2 shows that in the approach proposed in the present paper, for a 4-bit resolution SAR-ADC, each state is encoded into six bits. The two right-most bits (in grey) count the layer (e.g. they are "00" for the first layer and "10" for the second layer). The remaining four bits (in black) track the sequence of the comparator outputs. In the initial state, these bits are all set to "1". After each comparison, these bits are right-shifted and the left-most one is replaced by the comparator outcome.

In the general case of an R-bit resolution ADC, the right-most bits in grey are in the number of the next higher integer of $\log_2 R$ and the remaining bits in black are in the number of R.

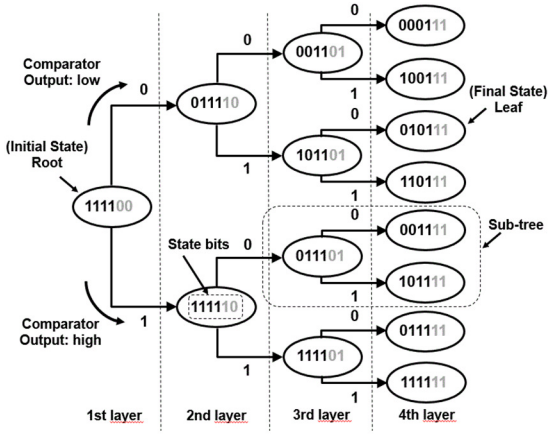

Fig. 2. State transition diagram for the DCL.

3. DCL architecture and schematics

The state encoding described in the previous section does not minimize the number of bits for the design of the finite state machine. In fact, four bits would be indeed enough to encode the fifteen states in Figure 2. The advantage offered by the proposed state encoding is that the next state of the binary algorithm can be generated from the actual one by using a shift register for the bits in black and a counter for the bits in grey, making straightforward, in this way, the design of the DCL. The resulting architecture of the DCL is depicted in Figure 3.

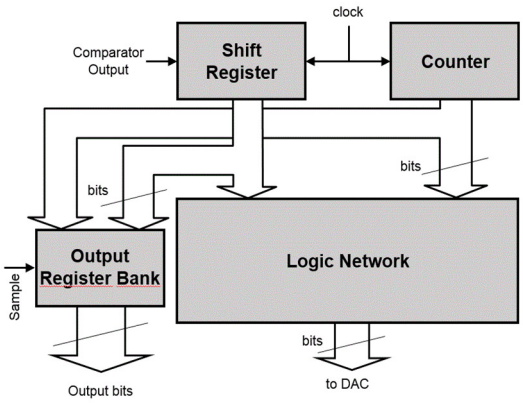

Fig. 3. Building block diagram of the DCL.

It is constituted by four main building blocks: a shift register, a counter, a logic network, and an output register bank. Note that no sequencers and code registers are used. The shift register can be obtained by cascading four D-type registers as depicted in the

following Figure 4a. The counter can be implemented as a binary counter obtained by arranging two D-type registers as in Figure 4b. Eventually, the output register bank is an array of four D-type registers as sketched in Figure 4c. In the case of a 4-bit resolution SAR-ADC, the design of the DCL requires therefore a total of ten D-type registers. The D-type register is therefore the basic cell to build up the DCL. In the present work, this register was designed by arranging in a master-slave configuration two transmission gates based latches, as depicted in the following Figure 5.

Figure 4 shows the ten D-type registers used in the case of a 4-bit resolution SAR-ADC. For a higher resolution R, the DCL can be quickly re-designed by just extending the register chains in Figure 4. This consideration highlights the simplification in the design of the DCL allowed by the sub-optimal state encoding described in Figure 2. The shift register and the output register bank, each needs a chain of R D-type registers and the binary counter needs a chain with a number of D-type registers equal to the next higher integer of $\log_2 R$. In the case of an R-resolution SAR-ADC the design of the DCL requires therefore a total of $2R+ \log_2 R$ registers.

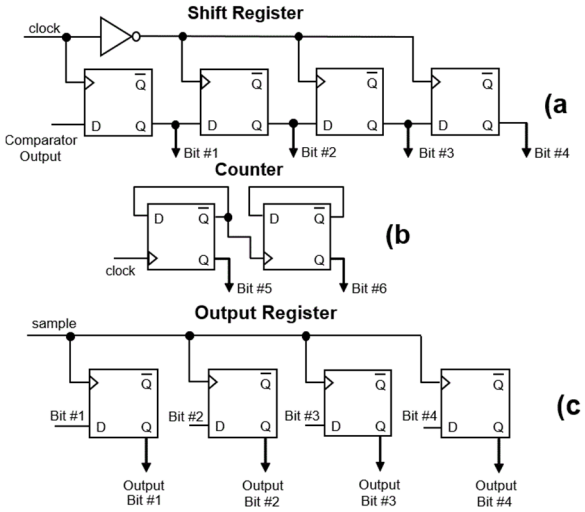

Fig. 4. Schematics of the shift register, the counter, and the output register bank in the case of a 4-bit SAR-ADC.

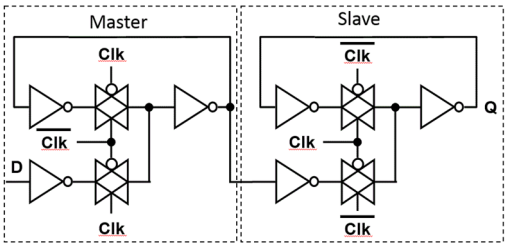

Fig. 5. Schematic of the D-type register.

The state encoding bits, as generated by the shift register and the binary counter, cannot be used directly to control the DAC. The logic network in Figure 3 is in charge of translating the state encoding bits into signals useful to control the DAC. The design of this logic network depends therefore on both the implementation of the DAC and the specific architecture of the SAR-ADC.

4. 8-bit resolution SAR-ADC

The previously described idea of DCL was applied to the design of an 8-bit resolution 130nm CMOS SAR-ADC, whose architecture is depicted in the following Figure 6. As in the case of the general architecture in Figure 1, it uses one comparator and one DCL but, as a difference, it uses two DACs instead of only one. With the DAC implemented in the form of a switching capacitor network, as depicted in the following Figure 7, this architecture allows for the minimization of the dissipated energy [2]. The use of two DAC's leads to a different way of using the comparator. In the general architecture the comparator receives the sampled value of the analog input signal V_{IN} to be digitized (see Figure 1) while in the architecture in Figure 6 V_{IN} is sampled by the DAC2 when the signal Sample is active. The comparator compares the voltages at the node Y and Z generated by the two DACs.

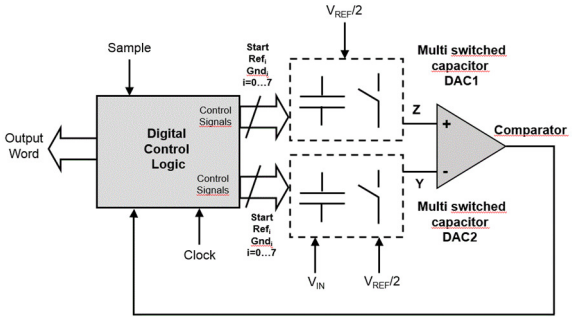

Fig. 6. Architecture of the designed 8-bit SAR-ADC.

For the architecture in Figure 6, the logic network, has been designed to implement the following switching strategy. During the sample phase, the capacitors in the DAC1 are discharged with both plates at the potential $V_{REF}/2$, where V_{REF} is the reference voltage used for the conversion process, while the capacitors in DAC2 are charged at V_{IN}-$V_{REF}/2$. In the following phase, all Ref_i signals are forced to 1 and Gnd_i signals to 0. This phase generates the Most Significant Bit (MSB). The comparator outcome is used by the DCL to generate the future control signals for the two DACs. In particular, at the n-th comparison phase, the signal Ref_n is forced equal to the comparator outcome and the signal Gnd_n equal to inverse of the comparator outcome. At the same time, the signal Ref_{n-1} is forced to zero and the signal Gnd_{n-1} to one. In this way, comparison by comparison the DCL explores the binary tree of Figure 2 until the Least Significant Bit (LSB) is generated. For an 8-bit resolution SAR-ADC the logic network receives

therefore eleven ($8+\log_2 8$) bits from the shift register and the binary counter and generates sixteen control signals Ref_i and Gnd_i (i=0…7). The logic network was synthesized through Karnaugh's maps and designed by using static NOR and NAND CMOS logic gates.

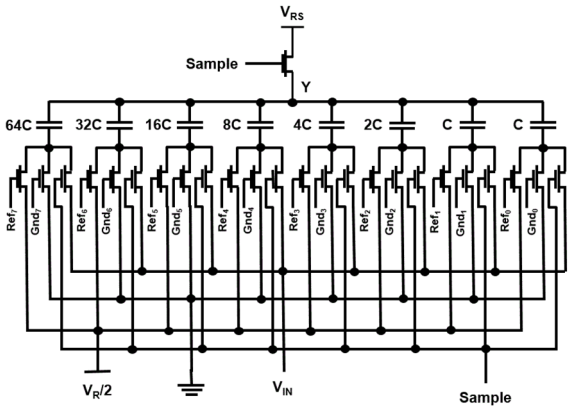

Fig. 7. Schematic of the DAC for the designed 8-bit SAR-ADC.

The comparator was designed as a dynamic latch, because of its higher sensitivity and lower dissipated power with respect to an operational amplifier based solution. Figure 8 depicts the schematic of the designed dynamic latch comparator. Since the circuit is very sensible to capacitive mismatches at the output nodes, a dummy inverter was added at the output node of the comparator not connected to the DCL.

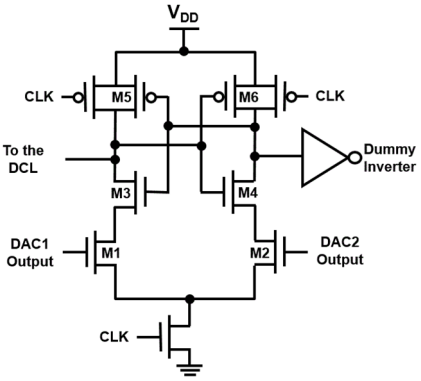

Fig. 8. Schematic of the dynamic latch comparator.

5. Simulations

As a first simulation, a sinusoidal tone with an amplitude of 800mVpp and an oscillation frequency of 70Hz was applied at the input of the designed SAR-ADC. The sampling frequency was set equal to 1.4kS/s, the clock signal to 12.5kHz, and V_{REF} to 800mV. The following Figure 9 shows a 12ms time interval of the input signal. The figure highlights on the input waveform six samples (samples #2, #6, #9, #11, #13, and #16), whose values are reported in Table I. Figure 10 shows how the output bits are generated during the time for each of the previous six samples.

For example, the input sample #2, sampled in correspondence of the sampling pulse #2, is digitized during the time interval between this sampling pulse and the following sampling pulse #3. The output bits are made available in correspondence of the rising edge of the sampling pulse #3. It is therefore visible a latency time, spent by the DCL for exploring the binary tree (see Figure 2) during the digitization process.

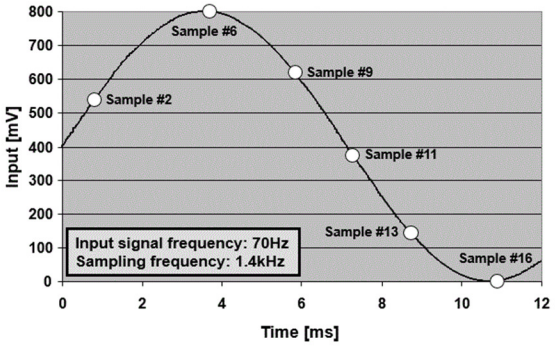

Fig. 9. Sampled values on the input sinusoidal waveform.

Table I. Output words and quantization error.

Sample	V_{IN}, (mV)	Output Word	V_A, (mV)	ΔV, (mV)
#2	537.790	10101100	537.50	0.29
#6	799.560	11111111	796.88	2.69
#9	617.310	11000101	615.63	1.69
#11	374.780	01111000	375.00	0.22
#13	143.500	00101110	143.75	0.25
#16	1.120	00000000	0.000	1.12

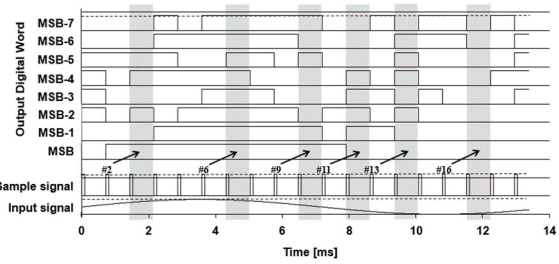

Fig. 10. Generation of the output digital word.

Table I reports also the voltage V_A computed from the output digital word using the usual formula:

$$V_A = V_{REF} \sum_{i=0}^{7} \frac{MSB - i}{2^{i+1}} \qquad (1)$$

where MSB-i is the i-th output bit, being MSB-0 the MSB and MSB-7 the LSB. The most-right column in Table I shows the quantization error ΔV between V_{IN} and V_A. It is possible to observe that ΔV is always lower than one LSB (3.13mV). Table I provides therefore a first rough indication that the designed SAR-ADC is correctly working.

The performances of the designed SAR-ADC were more in depth tested by investigating the static parameters Differential Non-Linearity (DNL) and Integral Non-Linearity (INL), and the dynamic parameters Equivalent Number of Bit (ENOB), Signal-to-Noise Ratio (SNR), Total Harmonic Distortion (THD), and Signal-to-Noise And Distortion ratio (SINAD), as well. The simulation set-up employed for these parameters are shortly sketched in the following Figure 11. The ideal DAC was described in Verilog-A code. For INL and DNL (upper part of the figure) a slow linear voltage ramp covering the whole input dynamic range was applied at the input of the SAR-ADC under test. The stair-case ramp generated by the Verilog-A code DAC was analyzed in the time domain by investigating the distribution of the thresholds. The following Figures 12 and 13 show the obtained DNL and INL, respectively.

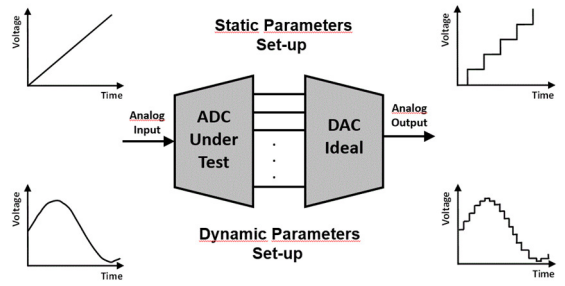

Fig. 11. Simulation set-ups for static and dynamic parameters of the SAR-ADC.

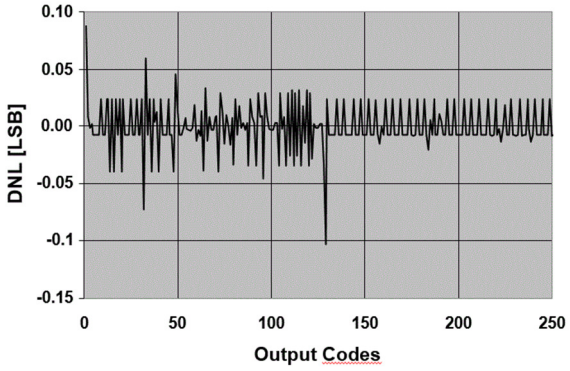

Fig. 12. Differential Non-Linearity of the designed SAR-ADC.

The DNL oscillates in the +/-0.05LSB range with exception for the code #128, where it exhibits a peak at around -0.1LSB. The worst DNL can be indeed expected when the MSB changes [7]. The INL is in the -0.15LSB/+0.10LSB range with a step in correspondence of the worst DNL.

For ENOB and SNR (lower part of Figure 11) a 70Hz sinusoidal tone was applied at the input and the stair-case waveform generated by the ideal DAC was analyzed in the frequency domain with a Discrete Fourier Transform. The following Figure 14 shows the spectrum. The summation of the first eleven harmonics leads to a THD of 45.9dB. By accounting for the process gain from the noise floor it is possible to compute a SNR of about 42.9dB.

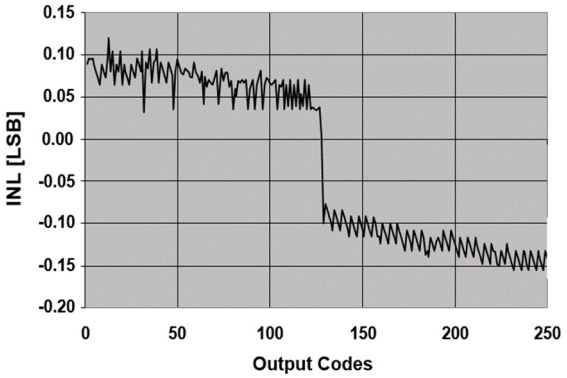

Fig. 13. Integral Non-Linearity of the designed SAR-ADC.

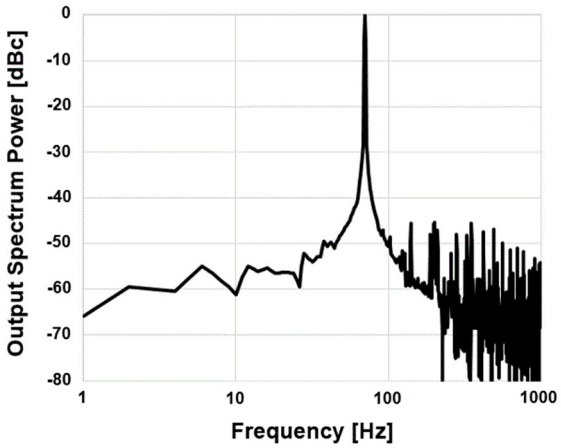

Fig. 14. Spectrum of the stair-case sinusoidal tone generated by the ideal DAC in the simulation set-up for dynamic parameters.

The following equation (2) allows for computing the SINAD:

$$SINAD = -10log\left(10^{-\frac{THD}{10}} + 10^{-\frac{SNR}{10}}\right) \qquad (2)$$

which results to be 41.2dB. Finally, through the following equation (3) it is possible to compute the ENOB:

$$ENOB = \frac{SINAD - 1.76}{6.02} \qquad (3)$$

which results to be 6.5 bits.

THD can be also estimated from the INL through the following equation (4) [8]:

$$THD = 20log\frac{INL_{MAX}}{2^{N-1}} \qquad (4)$$

where INL_{MAX} is the maximum observed module of INL and N is the number of bits. Since INL_{MAX}=0.15LSB from Figure 13 and N=8 for the designed SAR-ADC, the equations from (2) to (4) provide therefore an ENOB of 6.8bits. It is therefore

possible to estimate an ENOB of 6.65 bits for the SAR-ADC proposed in the present work.

Table II compares the obtained DNL, INL and ENOB with those reported of other 130nm CMOS SAR-ADCs in the literature. The present SAR-ADC well compares with the literature even if it suffers from a somewhat low ENOB.

Table II. Output words and quantization error.

	[9]	[10]	[11]	This work
Resolution [bits]	8	10	8	8
DNL [LSB]	+/- 0.61	-0.61 / +0.54	-0.15 / +0.15	-0.05 / +0.05
INL [LSB]	+/- 0.63	-0.46 / +0.45	-0.35 / +0.23	-0.15 / +0.10
ENOB [bits]	7.6	9.1	7.8	6.7

The following Figure 15 plots the dissipated power versus the sampling rate for several SAR-ADC collected in the literature regardless of the employed technology. The two dashed lines in the figure suggest that the power dissipated (P_D) by the SAR-ADC increases of 10dB when the sampling frequency increases of one decade. Figure 15 shows that the SAR-ADC proposed in the present work (open symbol in the figure) well compares with the literature.

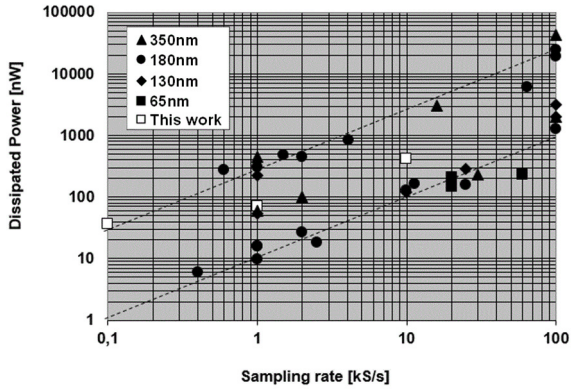

Fig. 15. Dissipated power versus sampling rate. References for 350nm: [2], [12]-[16]. References for 180nm: [2], [17]-[27]. References for 130nm [10], [11], [28]-[31]. References for 65nm: [32]

A more homogeneous comparison with the state-of-the-art in the literature can be carried out through the following Figure-of-Merit (FoM) [11], [14]:

$$FoM = \frac{P_D}{f_s 2^{ENOB}} \qquad (5)$$

It quantifies the energy dissipated to complete a conversion step. The following Figure 16 plots this FoM versus the sampling rate for the SAR-ADCs already addressed in the previous Figure 15. Even if with a FoM somewhat higher than the average value, the SAR-ADC described in the present work still remains comparable with other SAR-ADCs reported in the literature.

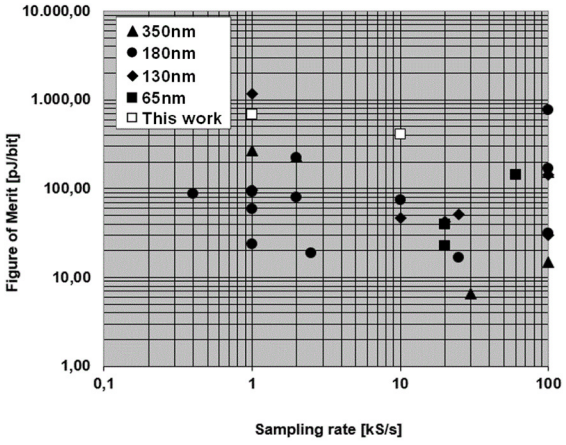

Fig. 16. FoM versus sampling rate. References for 350nm:[2], [12]-[16] References for 180nm: [2], [17]-[27]. References for 130nm [10], [11], [28]-[31]. References for 65nm: [32]

6. Conclusions

The present paper proposes the design of a low complexity digital control circuitry for SAR-ADC. The elementary cell for the design of this control circuitry is a D-type register. The obtained control circuitry results to be of low complexity. It is indeed constituted by two chains of registers, whose lengths can be easily accommodated to the desired resolution.

The proposed digital control circuitry was applied to the design of an 8-bit resolution SAR-ADC in a 130nm CMOS bulk technology. The simulations demonstrated that the designed SAR-ADC correctly works exhibiting performances well comparable with the literature in terms of DNL, INL, and dissipated power. The only weakness was the ENOB, which results to be less performant without nevertheless severely affecting the energy spent per bit generation that remains comparable with the literature.

Acknowledgements

The authors would like to acknowledge STMicroelectronics for providing the 130nm CMOS technology Design Kit. The technical contribution of Luca Toni is also warmly acknowledged.

References

[1] T.O.Anderson, Optimum Control Logic for Successive Approximation Analog-to-Digital Converters, in *The Deep Space Network Progress Technical Report*, November-December, 1972, pp.168-176.

[2] W. Hu, Y-T. Liu, T. Nguyen, D.Y.C. Lie, B.P. Ginsburg, An 8-bit Single-Ended Ultra-Low-Power SAR ADC With a Novel DAC Switching Method and a Counter-Based Digital Control Circuit, *IEEE Transactions on Circuits and Systems – I, Regular papers*, Vol. 60, Issue 7, 2013, pp. 1726-1739.

[3] H.T. Russel, An Improved Successive-Approximation Register Design for Use in A/D Converters, *IEEE Transactions on Circuits and Systems*, Vol. 25, Issue 7, 1978, pp. 550-554.

[4] A. Rossi, G. Fucili, Non-redundant successive approximation register for A/D converters, *Electronics Letters*, Vol. 32, Issue 12, 1996, pp. 1055-1057.

[5] M.D. Scott, B.E. Boser, K.S.J. Pister, An Ultralow-Energy ADC for Smart Dust, *IEEE Journal of Solid-State Circuits,* Vol. 38, Issue 7, 2003, pp. 1123-1129.

[6] M.Borgarino, N.Verrascina, J-B.Begueret, Simplified Design of the Digital Control Logic for SAR-ADC, in *International Conference on Microelectronic Devices and Technologies (MicDAT2018)*, Barcelona, Spain, 20-22 June 2018, pp. 1-4.

[7] P.Xiaomin, Z.Jun, Design and Optimization of the Interior DAC of SAR ADC, in *Proceedings of the International Conference on 'Information Management and Engineering (ICIME 2011)'*, Toronto, Canada, 27-28 April 2011, pp. 1-7.

[8] A.Buchwald, Specifying and Testing ADCs Video, in *Short Course and Tutorials of the International Solid-State Circuits Conference (ISSCC)*, San Francisco, USA, 7-11 February 2010.

[9] S. Al-Ahdab, R.Lofti, W.A.Serdijn, A 1-V 225-nW 1KS/s Current Successive Approximation ADC for Pacemakers, in *Conference on Ph.D. Research in Microelectronics & Electronics*, Berlin, Germany, 18-21 July 2010, pp. 1-4.

[10] D.Zhang, A.Bhide, A.Alvandpour, A 53-nW 9.12 ENOB 1-kS/s SAR ADC in 0.13um CMOS for Medical Implant Devices, in *Proceedings of the European Solid-State Circuits Conference (ESSCIRC)*, 12-16 September 2011, Helsinki, Finland, pp. 467-470

[11] X.Yan, L. Fu, J. Wang, An 8-bit 100KS/s Low Power Successive Approximation Register ADC for Biomedical Applications, in *International Conference on ASIC*, 28-31 October 2013, Shenzhen, China, pp. 1-4.

[12] X.Zou, X.Xu, L.Yao, Y.Lian, A 1-V 450-nW Fully Integrated Biomedical Sensor Interface Chip, *IEEE Journal of Solid-State Circuits*, Vol. 44, Issue 4, 2009, pp. 1067-1077.

[13] X.Xu, X.Zou, L.Yao, Y.Lian, A 1-V 450-nW Fully Integrated Biomedical Sensors Interface Systems, in *IEEE Digest of Technical Paper Symposium on VLSI Circuits*, Honolulu, USA, 17-19 June 2008, pp. 78-79.

[14] L.Zheng, L.B.Leene, Y.Liu, T.G.Constandinou, An Adaptive 16/64kHz, 9-bit SAR ADC with Peak-Aligned Sampling for Neural Spike Recording, in *IEEE International Symposium on Circuits and Systems*, Melbourne, Australia, 1-5 June 2014, pp. 2385-2388.

[15] R.H.Gudlavalleti, S.C.Bose, Ultra Low Power 12-Bit SAR ADC for Wireless Sensing Applications, in *IEEE International Conference on VLSI Systems, Architectures, Technology and Applications (VLSI-SATA)*, Bangalore, India, 10-12 January 2016, pp. 1-4.

[16] S.Brenna, A.G.Bonfanti, A 70.7-dB SNDR 100-kS/s 14-b SAR ADC with attenuation capacitance calibration in 0.35-um CMOS, in *Analog Integrated Circuits and Signal Processing Journal*, Vol. 89, Issue 2, 2016, pp. 357-371.

[17] H.Zhang, Y.Qin, S.Yang, Z.Hong, Design on an Ultra-low Power SAR ADC for Biomedical Applications, in *IEEE International Conference on Solid-State and Integrated Circuits Technology*, Shangai, China, 1-4 November 2010, pp. 460-462.

[18] Y.K.Yang, X.Liu, J.Zhou, J.H.Cheong, M.Je, W.L.Goh, A 0.5V 16nW 8.08-ENOB SAR ADC for Ultra-Low Power Sensor Applications, in *IEEE Int. Microwave Workshop Series RF and Wireless Technologies for Biomedical and Healthcare Applications*, Singapore, Singapore, 9-11 December 2013, pp. 1-4.

[19] I. Kianpour, Z. Zou, M.B. Nejad, L.R. Zheng, An 8-bit 166nW 11.25 kS/s 0.18um two-Step-SAR ADC for RFID applications Using Novel DAC Architecture, in *IEEE NORCHIP Conference*, Tampere, Finland, 15-16 November, 2010, pp. 1-4.

[20] A.T. Do, C.K. Lam, Y.S. Tan, K.S. Yeo, J.H. Cheong, L. Tao, M.T. Tan, M. Je, A 9.87 nW 1 kS/s 8.7 ENOB SAR ADC for Implantable Epileptic Seizure Detection Microsystems, in *IEEE Asia and Pacific Conference on Circuits and Systems*, Kaohsiung, Taiwan, 2-5 December 2012, pp 1-4.

[21] R.Sekimoto, A.Shikata, H.Ishikuro, A Power Scalable SAR-ADC in 0.18um-CMOS with 0.5V Nano-Watt Operation, in *IEEE International Symposium on Access Spaces (ISAS)*, Yokohama, Japan, 17-19 June 2011, pp. 89-94.

[22] H.Zhang, Y.Qin, Z.Hong, A 1.8-V 770-nW Biopotential Acquisition System for Portable Applications, in *IEEE Biomedical Circuits and Systems Conference*, Beijing , China, 26-28 November 2009, pp. 93-96.

[23] N.Verma, A.P.Chandrakasan, An Ultra Low Energy 12-bit Rate-Resolution Scalable SAR ADC for Wireless Sensor Nodes, *IEEE Journal of Solid-State Circuits*, Vol. 42, Issue 6, 2007, pp. 1196-1205.

[24] Y.Susanti, P.K.Chan, V.K.S.Ong, An Ultra Low-Power Successive Approximation ADC Using an Offset-Biased Auto-Zero Comparator, in *IEEE Asia Pacific Conference on Circuits and Systems*, Macao, China, 30 November – 03 December, 2008, pp. 284-287.

[25] A.T.Do, C.K.Lam, Y.S.Tan, K.S.Yeo, J.H.Cheong, X.Zou, L.Yao, K.W.Cheng, M.Je, A 160 nW 25 kS/s 9-bit SAR ADC for neural signal recording applications, , in *IEEE International Conference on New Circuits and Systems*, Montreal, Canada, 17-20 June 2012, pp. 525-528.

[26] S.K.Lee. S.J.Park, Y.Suh, H.J. Park, J.Y. Sim, A 1.3uW 0.6V 8.7-ENOB Successive Approximation DAC in a 0.18um CMOS, in *IEEE Digest Technical Papers Symposium on VLSI Circuits*, Kyoto, Japan, 15-18 June 2009, pp. 242-243.

[27] J.Sauerbrey, D.Schmitt-Landsiedel, R.Thewes, A 0.5-V 1-uW Successive Approximation ADC, *IEEE Journal of Solid-State Circuits*, Vol. 38, Issue 7, 2003, pp. 1261-1265.

[28] P.Kamalinejad, S.Mirabbasi, V.C.M.Leung, An Ultra-Low-Power SAR ADC with an Area-Efficient DAC

Architecture, in *IEEE International Symposium on Circuits and Systems*, Rio de Janeiro, Brazil, 15-18 May 2011, pp. 13-16.

[29] K.Abdelhalim, L.MacEachern, S.Mahmoud, A Nanowatt ADC for Ultra Low Power Applications, in *IEEE International Symposium on Circuits and Systems*, Kos, Greece, 21-24 May 2006, pp. 1507-1510.

[30] K.Abdelhalim, L.MacEachern, S.Mahmoud, A Nanowatt Successive Approximation ADC with Offset Correction for Implantable Sensor Applications, in *IEEE International Symposium on Circuits and Systems*, New Orleans, USA, 27-30 May 2007, pp. 2351-2354.

[31] A. Rodriguez-Perez, M.Delgado-Restituto, J.Ruiz-Amaya, F.Medeiro, An Ultra-Low Power Consumption 1-V, 10-bit Successive Approximation ADC, in *IEEE International Conference on Electronics, Circuits and Systems*, St. Julien's, Malta, 31 August-03 September 2008, pp. 634-637

[32] M.Yip, A.P.Chandrakasan, A Resolution-Reconfigurable 5-to-10b 0.4-to-1V Power Scalable SAR ADC, in *IEEE International Solid-State Circuits Conf*erence, San Francisco, USA, 20-24 February 2011, pp. 190-192.